



# T-Mamba: A unified framework with Long-Range Dependency in dual-domain for 2D & 3D Tooth Segmentation

Jing Hao<sup>1</sup>, Yonghui Zhu<sup>2</sup>, Lei He<sup>3</sup>, Moyun Liu<sup>3</sup>, James Kit Hon Tsoi<sup>1</sup>, and Kuo Feng Hung<sup>1, \*</sup>

<sup>1</sup>The University of Hong Kong, Hong Kong SAR, China

<sup>2</sup>Imperial College London, UK

<sup>3</sup>Huazhong University of Science and Technology, China

\*Corresponding author: [hungkfg@hku.hk](mailto:hungkfg@hku.hk)

## Abstract

Tooth segmentation is a pivotal step in modern digital dentistry, essential for applications across orthodontic diagnosis and treatment planning. Despite its importance, this process is fraught with challenges due to the high noise and low contrast inherent in 2D and 3D tooth data. Both Convolutional Neural Networks (CNNs) and Transformers has shown promise in medical image segmentation, yet each method has limitations in handling long-range dependencies and computational complexity. To address this issue, this paper introduces T-Mamba, integrating frequency-based features and shared bi-positional encoding into vision mamba to address limitations in efficient global feature modeling. Besides, we design a gate selection unit to integrate two features in spatial domain and one feature in frequency domain adaptively. T-Mamba is the first work to introduce frequency-based features into vision mamba, and its flexibility allows it to process both 2D and 3D tooth data without the need for separate modules. Also, the TED3, a large-scale public tooth 2D dental X-ray dataset, has been presented in this paper. Extensive experiments demonstrate that T-Mamba achieves new SOTA results on a public tooth CBCT dataset and outperforms previous SOTA methods on TED3 dataset. The code and models are publicly available at <https://github.com/isbrycee/T-Mamba>.

**Keywords:** Tooth Segmentation, Vision Mamba, Frequency Feature Modeling, Deep Learning.

## 1. Introduction

The evolutionary key of modern digital dentistry lies in the acquisition and delineation of oral regions in different types of tooth data, including 2D panoramic radiography and 3D CBCT image. This technology finds several uses in oral and maxillofacial disciplines, including orthodontic diagnosis and treatment planning K. F. Hung et al., 2022, 2023; K. Hung et al., 2020. Tooth segmentation is a crucial step in digital workflows, involving the extraction of a cluster of voxels from 3D digital models along with their intensity and density information, or the delineation of tooth regions from 2D grayscale panoramic radiographs. The process of tooth segmentation is critical

in dental diagnostics, because it plays a key role in assessing conditions like impacted teeth, superordinate teeth, and missing dentition. Additionally, it aids in the review and evaluation of orthodontic treatment outcomes Hou et al., 2023. However, an accurate tooth segmentation process is challenging for several reasons. First of all, either the 2D panoramic radiography or 3D digital model is hard to observe due to the natural property of high noise and low contrast. In addition, the presence of metal fillings and prosthetic restorations in tooth image data introduces artifacts that induce distortions, significantly complicating the identification of teeth. Finally, the tooth data is typically acquired in natural occlusion, posing challenges in distinguishing between lower and upper teeth due to their similar densities.

Deep learning has been widely used in the field of medical image segmentation, and many researchers are dedicated to employing deep learning techniques for automated segmentation of tooth Chen et al., 2023; Cui et al., 2019, 2021; Yin et al., 2023. CNNs and Transformers architecture have displayed considerable promise in medical image segmentation due to their ability to learn complex image features, but both of them have limited ability to handle long-range dependencies because of inherent locality or computational complexity. The CNNs can only capture translational invariances and extract local features, and the Transformer is struggled by the heavy computational complexity when capturing global contextual information. Due to their complementary feature, many studies have explored incorporating Transformers into CNNs via hybrid network architectures. Nonetheless, the obvious shortcoming of Transformers is resource-intensive because the self-attention mechanism scales quadratically with the input size and poses challenges in terms of speed and memory usage with high-resolution biomedical images. While substantial effort has been dedicated to reducing the computational complexity of Transformers, they often come at the expense of sacrificing model accuracy Maaz et al., 2022; Zhai et al., 2023. Therefore, the efficient enhancement of long-range dependency in CNNs continues to be an unresolved issue.

Recently, motivated by the success of Mamba in language modeling, many studies have transferred this success from language to vision for the aim of achieving linear complexity without sacrificing global receptive fields Y. Liu et al., 2024; Zhu et al., 2024. However, we identify two limitations in utilizing vision mamba to assist CNNs for modeling long-range dependency. First and foremost, due to the inherent imaging principles of medical images such as CT and X-ray, these images possess natural attributes of high noise and low contrast from a visual perspective. For such images, frequency domain-based feature representations are more accurate, unique, and robust. However, CNNs and vision mamba models typically extract semantic features solely from the spatial domain, overlooking the rich frequency domain-based information. As indicated by Azad et al., 2021, high-frequency components capture texture details, whereas low-frequency components encode shape information. Therefore, integrating frequency domain features with spatial domain representations holds promise for enhancing the image feature extraction in medical images, consequently improving the accuracy of prediction. Secondly, CNNs can process 2D or 3D features directly while vision mamba structures is to handle 1D feature sequences. In the CNN and vision mamba hybrid architecture, the transformation of features by vision mamba inevitably leads to the loss of spatial position information. This spatial context is crucial, particularly in tasks requiring dense precise positional prediction.

Inspired by these two limitations, we design a network named T-Mamba, which amalgamates our proposed Tim (Tooth Vision Mamba) block with DenseVNet Gibson et al., 2018 in multi-

scale features, for tooth image segmentation. The Tim block exhibits three key strengths: (1) It extracts image features in both frequency domain and spatial domain, thus we can derive more accurate, unique, and robust feature representations for medical images which are of high noise and low contrast. Based on the attributes of features at different scales, we have employed distinct bandpass filtering strategies tailored to each scale. (2) It contains a shared bi-position embeddings which are to compensate for the positional information lost during reshape operation. It is noteworthy that we employ a singular positional embedding within each feature-scale. This not only guarantees the preservation of spatial positions across feature maps of identical scales but reduces model parameters and computational burden. (3) It includes a gate selection unit for integrating two features in spatial domain (both forward and backward directions) and one feature in frequency domain adaptively. The gate selection unit is data-dependent and can assign weights for three distinctive features according to input sequence tokens. Also, Our T-Mamba demonstrates the superior flexibility when processing 2D and 3D tooth data, without the need for separate, carefully designed modules for each type of data. When extracting feature for different types of data, changing the dimension of CNN is adequate because the Tim block in the T-Mamba transforms the input data into 1D sequences for feature modeling. Therefore, T-Mamba provides a unified solution with long-range dependency for both 2D and 3D tooth segmentation.

In order to verify the effectiveness of T-Mamba, extensive experiments were conducted on both 3D tooth CBCT data and 2D tooth X-ray images. Due to the unavailability to a large-scale 2D tooth X-ray datasets, we build the TED3 dataset, a public Teeth large-scale 2D X-Ray Dental Dataset. This dataset is entirely based on the collection and integration of various publicly available panoramic dental X-ray datasets accessible online. It consists of 6225 labelled data and 14728 unlabelled data, which is the largest 2D tooth X-ray segmentation dataset to date.

Our T-Mamba outperforms previous state-of-the-art results in a large margin on a public 3D tooth CBCT dataset and our TED3 dataset. Besides, we also implement sufficient ablation studies to verify the effectiveness of three components in our proposed Tim block. To the best of our knowledge, T-Mamba is the pioneering effort to incorporate frequency domain features into the vision mamba framework. Our main contributions can be summarized as follows: Our main contributions can be summarized as follows:

- We propose T-Mamba, which incorporates our designed Tim block with DenseVNet for global and local visual context modeling for both 2D & 3D Tooth segmentation.
- The Tim block is the first work to extract more robust and unique representations for medical images which are of high noise and low contrast by introducing frequency-based features.
- We introduce a large-scale 2D tooth X-ray segmentation dataset, TED3, which consists of 6225 labelled data and 14728 unlabelled data.
- Without bells and whistles, T-Mamba achieves new SOTA results on the public Tooth CBCT dataset and outperforms previous SOTA methods in a large margin on our proposed TED3 dataset.

## 2. Related Works

**Vision mamba and its variants.** Nguyen et al., 2022 is the first work applying SSMS into visual tasks and showing the potential that its performance may compete with ViT Dosovitskiy et al., 2020. Y. Liu et al., 2024 traverse the spatial domain and convert any non-causal visual image into order patch sequences. Zhu et al., 2024 marks the image sequences with position embeddings and compresses the visual representation with bidirectional SSMS. Yang et al., 2024 introduces the structured SSMS with spatiotemporal selective scan for medical video object segmentation task. Ma et al., 2024 which is a hybrid CNN-SSM architecture is proposed handle the long-range dependencies in biomedical image segmentation. In addition, there are some other works that leverage the SSMS into the medical image analysis field, point cloud analysis and vedio generation, such as Gao et al., 2024; Liang et al., 2024; C. Liu et al., 2024; J. Liu et al., 2024; Ruan & Xiang, 2024; Xing et al., 2024; Ye & Chen, 2024.

**3D Tooth CBCT Segmentation.** Accurate and automatic depiction of individual teeth from CBCT images is a critical step to assist physicians in the diagnosis and treatment of oral diseases. Cui et al., 2019 was the first to use neural networks to achieve automatic tooth segmentation and identification from CBCT images. Cui et al., 2021 was designed for robust and efficient tooth segmentation on 3D dental scanned point cloud data. Jang et al., 2021 present a fully automated method of identifying and segmenting 3D individual teeth by hierarchical multi-step models. Chen et al., 2023 designed a U-shaped network which combines the advantages of CNN and Transformer for dental CBCT images segmentation. Yin et al., 2023 proposed a context-transformed architecture and obtained better performance in tooth CBCT segmentation.

**2D Tooth X-Ray Segmentation.** Accurate segmentation of teeth in panoramic dental X-rays is also another challenging task due to variations in tooth morphology and overlapping regions. Rubiu et al., 2023a utilized a mask region-based convolutional neural network (Mask-RCNN He et al., 2017) to segment tooth instances in Panoramic Dental X-ray. Silva et al., 2020a brought a thorough study on tooth segmentation and numbering on panoramic X-ray images by means of end-to-end deep neural networks. Hou et al., 2023 proposed the Teeth U-Net by introducing context semantics and contrast enhancements upon U-Net. Haghanifar et al., 2023 proposed an automatic diagnosis system to detect dental caries in Panoramic images, using ensemble transfer learning and capsule classifier. Lin et al., 2023 designed a novel lightweight neural network scheme using knowledge distillation for dental X-ray image segmentation for the purpose of deployment on edge devices. However, these neural networks are specifically designed for 2D tooth data and cannot be directly applied to 3D tooth CBCT segmentation tasks, thus lacking a certain degree of flexibility. Our framework, on the other hand, can perform segmentation tasks on both 2D and 3D data without the need for carefully designed network structures specific to different data modalities.

## 3. Methodology

### 3.1 Preliminaries for Mamba

The advanced state space models (SSM), i.e., structured state space sequence models (S4) and Mamba, are a type of systems that maps a 1-D continuous function or sequence  $x(t) \in \mathbb{R} \mapsto y(t) \in \mathbb{R}$  through a hidden state  $h(t) \in \mathbb{R}^N$ . Mathematically, these models are typically formulated as

linear Ordinary Differential Equations (ODEs), as appears in (1):

$$\begin{aligned} h'(t) &= \mathbf{A}h(t) + \mathbf{B}x(t), \\ y(t) &= \mathbf{C}h(t), \end{aligned} \tag{1}$$

where the parameters include  $\mathbf{A} \in \mathbb{R}^{N \times N}$  as the evolution parameter, and  $\mathbf{B} \in \mathbb{R}^{N \times 1}$ ,  $\mathbf{C} \in \mathbb{R}^{1 \times N}$  as the projection parameters.

The SSM-based models, as continuous-time models, should be discretized when integrated into deep learning algorithms. This discretization transformation is crucial to align the model with the sample rate of the underlying signal embodied in the input data [1]. Given the input  $x(t) \in \mathbb{R}^{L \times D}$ , a sampled vector within the signal flow of length  $L$  following [2], Equation (1) could be discretized as follows using the Zeroth-Order Hold (ZOH) rule:

$$\begin{aligned} h_t &= \bar{\mathbf{A}}h_{t-1} + \bar{\mathbf{B}}x_t \\ y_t &= \bar{\mathbf{C}}h_t \\ \bar{\mathbf{A}} &= e^{\Delta\mathbf{A}} \\ \bar{\mathbf{B}} &= \Delta\mathbf{A}^{-1}(e^{\Delta\mathbf{A}} - \mathbf{I}) \cdot \Delta\mathbf{B} \\ \bar{\mathbf{C}} &= \mathbf{C}, \end{aligned} \tag{2}$$

where  $\Delta \in \mathbb{R}^D$  is the timescale parameter.

Eventually, the models compute output  $y$  through a global convolution operation within a structured convolutional kernel  $\bar{\mathbf{K}}$ :

$$\begin{aligned} \bar{\mathbf{K}} &= (\bar{\mathbf{C}}\bar{\mathbf{B}}, \bar{\mathbf{C}}\bar{\mathbf{A}}\bar{\mathbf{B}}, \bar{\mathbf{C}}\bar{\mathbf{A}}^2\bar{\mathbf{B}}, \dots, \bar{\mathbf{C}}\bar{\mathbf{A}}^{L-1}\bar{\mathbf{B}}), \\ y &= \bar{\mathbf{K}} \otimes y_t. \end{aligned} \tag{3}$$

### 3.2 T-Mamba architecture

We enhance the global representation dependency of CNN by leveraging Mamba’s linear scaling advantage with three optimizations, and propose a unified and powerful framework, T-Mamba, for 2D & 3D tooth semantic segmentation. The architecture of the T-Mamba is sketched in Fig. 1, which amalgamates our proposed Tim block with DenseVNet Gibson et al., 2018 in multi-scale features.

The T-Mamba adopts the classical single-stage V-shaped architecture, and consists of three feature scales. To enlarge the receptive field of CNN and model the long-range dependency, we simply insert the Tim block after each CNN layer in DenseVNet. Different from previous works that performing global feature extraction directly in the pixel space of medical images J. Liu et al., 2024; Ma et al., 2024; Xing et al., 2024, performing global modeling in a CNN-style feature space, which is with inductive bias property, is less challenging to optimize model parameters and yields better performance Z. Li et al., 2022; Tang et al., 2024; Xin et al., 2023.

T-Mamba can capture both localized fine-grained feature and long-range dependencies in terms of spatial domain and frequency domain for 2D tooth X-ray image or 3D tooth CBCT data. This implementation is achieved by simply modifying the type of CNN used for extracting features in T-Mamba, such as 2D convolution or 3D convolution. For 2D tooth X-ray images, 2D convolutional operations are used, while for 3D tooth CBCT data, 3D CNN convolutional

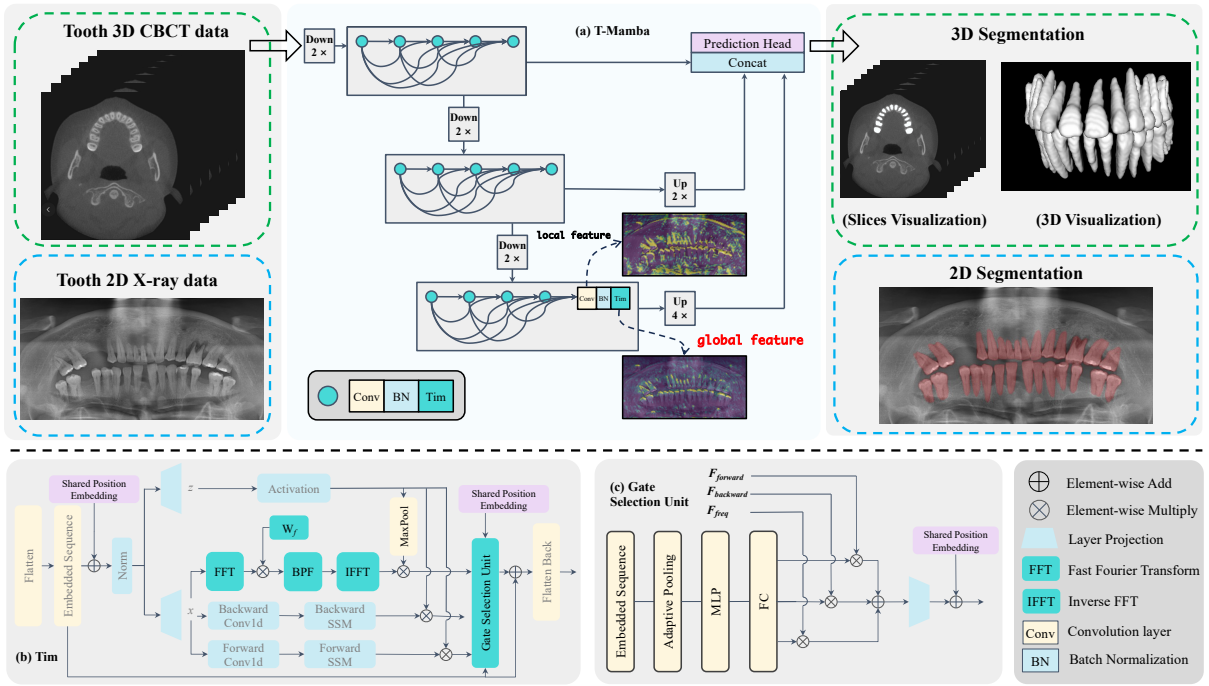


Figure 1: The framework of T-Mamba.

operations are employed. Note that our proposed Tim block does not require any modifications regardless of whether it is processing 2D or 3D data, as it transforms the input data into sequences for feature modeling. Therefore, our T-Mamba can flexibly perform feature modeling on both 2D and 3D data, without the need for meticulously designing different modules for various data modalities. After encoding the image features at three different scales, these features are concatenated together, and a lightweight prediction head is utilized to output the final segmentation results.

### 3.3 Tim block

The original Mamba block is devised for the 1-D sequence modeling, which is not compatible for vision tasks requiring spatial-aware understanding. The Vision Mamba Zhu et al., 2024 proposed Vim block which incorporates the bidirectional sequence modeling upon the Mamba block. However, directly applying this module to tooth modality data for feature modeling may yield suboptimal results due to the intrinsic differences between tooth data and natural images. Unlike natural images, tooth data typically comprises grayscale images with lower contrast and unclear object textures. Meanwhile, the Vim block neglects the spatial feature loss during the process of converting high-dimensional data into 1D sequential data. Motivated by these problems, we further enhance the Vim block by introducing three components for better the feature modeling of tooth modality data: 1) Frequency-based band pass filtering; 2) Shared bi-positional encoding compensation; 3) Gated selection unit. The Tooth Vision Mamba (Tim) block is shown in Fig. 1.

**Frequency-based band pass filtering.** The Fourier domain plays a major role in extracting frequency-based analysis of image information and it's evident that fine details and outlines could be captured in frequency domain even with poor quality X-ray Said et al., 2004; Y. Yu et al., 2021 and CT Azad et al., 2021; L. Li et al., 2024. The convolutional layers have a strong texture

inductive bias, and they tend to learn texture-based features. Representing an object in terms of frequency may reduce the effect of texture bias since only the high frequencies are responsible for the texture information (like boundaries) and lower frequencies might be related to the shape and outline. Zhou et al., 2023.

Inspired by this, we evolve the structure of Vim by enhancing features extraction in frequency domain. Specifically, we firstly transform the sequence features  $X$  to the Fourier domain, then extract frequency features using learnable weight parameters  $W_f$  and implement a bandpass filtering, and finally conduct the inverse Fourier transform to get the signal back. After that, the frequency feature is aggregated by the activated  $Z'$  with maxpooling operation. Since image information varies at different scales of features, we have applied specific frequency domain filtering operations to different scales of features. For low-level features, which primarily contain the shape and outline of objects, we perform low-pass filtering operations to enhance the modeling of object contours and shape. For high-level features, high-pass filtering is implemented to enhance the modeling of texture information in images. For medium-level features, we apply band-pass filtering operations accordingly.

The whole process can be formulated as:

$$\mathcal{F}_{freq} = IFFT(Bandpass(W_f(FFT(X)))) * Maxpool(Z'), \quad (4)$$

$$Bandpass = \begin{cases} X * (|X| < S_{low}), X \in low - level \text{ features}, \\ X * (S_{low} < |X| < S_{high}), X \in medium - level \text{ features}, \\ X * (|X| > S_{high}), X \in high - level \text{ features}, \end{cases} \quad (5)$$

where  $S_{low}$ ,  $S_{high}$  are the thresholds of bandpass filtering. In our experiments, we set  $S_{low}=0.1$  and  $S_{high} = 0.9$ . The low-level, medium-level, high-level indicates three different feature scales in our network, respectively.

**Shared Dual Positional Encoding Compensation.** Our T-Mamba network integrates the local feature extraction capabilities of convolutional layers with the SSMS for capturing the long-range dependency. Convolutional layers typically handle 2-D or 3-D feature maps, while our designed Tim block focuses on process 1-D sequences data. Consequently, reshaping high-dimensional features into 1-D feature tokens is essential. However, this process inevitably results in the loss of crucial positional information, which is vital for dense prediction tasks. To mitigate this, we employ position embeddings to compensate for the positional information lost during the reshape operation.

Specifically, given an input feature  $\mathcal{I}$  with a shape of  $(B, C, H, W, D)$ , we first flattened it to 1-D feature tokens with a shape of  $(B, L, C)$  where  $L = H \times W \times D$  and then add a learnable position embedding  $\mathcal{F}_{pos}$  with a shape of  $(C, L)$  to feature tokens to retain positional information.

$$X = Flatten(\mathcal{I}) + \mathcal{F}_{pos}, \quad (6)$$

where  $X$  is sequence features which is fed to our Tim block.

Regarding the output of Tim block, we also need to reshape the 1-D feature tokens into high-dimensional features for next convolutional operation. To further enhance the spatial information within the 1-D feature tokens, the positional embedding we used before is added to 1-D feature tokens again before reshaping them back into high-dimensional features. Note that the positional

embedding at each feature scale remains consistent. This practice ensures spatial positions remain unchanged in feature maps of the same scale, simultaneously reducing model parameters and computational burden. Following Vaswani et al., 2017, we initialize the position embedding via sinusoidal function:

$$\begin{aligned} PE_{(pos,2i)} &= \sin(pos/10000^{2i/d_{\text{model}}}), \\ PE_{(pos,2i+1)} &= \cos(pos/10000^{2i/d_{\text{model}}}), \end{aligned} \quad (7)$$

where pos is the position along with L and i is the index along with C.

We posit that adding a shared bi-positional embedding to both the input and output of the Tim block significantly preserves the positional information of high-dimensional features. Through ablation experiments, we validate that employing a shared bi-positional encoding leads to higher performance compared to using a single positional embedding.

**Gate Selection Unit.** The evolved Vim block consists of two features in spatial domain (both forward and backward directions) and one feature in frequency domain. We devise a Gate Selection Unit with the objective of fusing these distinctive features adaptively. The input embedding sequence is firstly down-sampled to a fixed dimension such as 2048, and it is projected through MLP (Multi linear projection), along with a fully connection to predict three proportions corresponding to three features. After that, the  $f_{fuse}$  is derived by weighted summation of three features and then projected by a linear layer, and Gate Selection Unit outputs the sum of the  $f_{fuse}$  and the residual information.

$$\begin{aligned} S_{forward}, S_{backward}, S_{freq} &= FC(MLP(Pooling(X))), \\ \mathcal{F}_{fuse} &= \sum (S_i * \mathcal{F}_i), i \in \{forward, backward, frequency\}, \\ O_{gate} &= \mathcal{F}_{fuse} + X. \end{aligned} \quad (8)$$

The Gate Selection Unit is data-dependent because the three weight coefficients are computed from source X, and these weight coefficients are then used to update different forms of features of X. Consequently, the Gate Selection Unit can adaptively adjust the combination of the three forms of features based on different inputs, thus obtaining a better feature representation.

## 4. TED3 Dataset

Table 1: Composition of our proposed TED3 dataset.

Dataset	Whole	Training Set	Test Set
TED3-labelled	6225	5000	1225
TED3-unlabelled		14728	

Currently, most deep learning-based tooth segmentation algorithms for panoramic radiographs are designed and validated on private dataset because of the data protection, privacy concerns and annotation cost Almalki & Latecki, 2023; Kanwal et al., 2023; Rubiu et al., 2023b; Sheng et al., 2023. This leads to the issue that most methods suffer from limited generalization ability due to the small training dataset size (typically less than 1000 images) and the lack of data diversity. Additionally, the majority of existing datasets are collected from the single



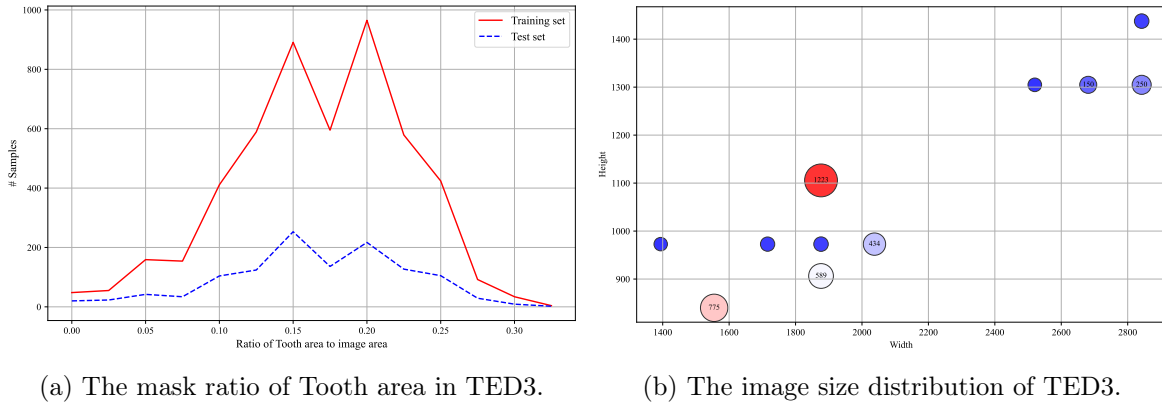


Figure 2: The detailed statistics of TED3

center, resulting in the overfitting of center-specific characteristics during model training and thus impeding the generalization to data from different centers. These limitations hinder the advancement of deep learning in the field of dentistry.

To solve this issue, we build the TED3 dataset, a public **T**eeth large-scale **2D X-Ray Dental Dataset**. This dataset is entirely based on the collection and integration of various publicly available panoramic dental X-ray datasets accessible online. Some small datasets originating from diverse health institutions for panoramic dental X-rays are available, so we systematically organize all these available public datasets, filter the identical data, and subsequently partition them into training and testing sets. We have compiled all publicly available panoramic dental X-ray datasets from the current online resources, with detailed information regarding their sources and dataset descriptions provided in the appendix. Table 1 provides an overview of TED3.

The TED3 consists of two parts: TED3-labelled data and TED3-unlabelled data. The TED3-labelled data includes 6225 images, with 5,000 training images and 1225 test images. TED3-labelled is an amalgamation of multiple publicly available datasets from the internet, resulting in the diversity ranging from imaging devices, patient ages, and dental conditions. Therefore, the test set of TED3-labelled data enables comprehensive validation of the model’s generalization ability, mitigating the risk of overfitting to a specific data distribution from a single health center. Figure 3 illustrates various samples in the test set, showcasing the diversity of test data distribution. Furthermore, we also provide the TED3-unlabelled data with 15069 unlabeled images. These data are primarily sourced from publicly available panoramic dental X-rays but lack binary masks. We believe that TED3-unlabeled data is beneficial for self-supervised learning and semi-supervised learning purposes, thereby further enhancing the accuracy of tooth segmentation models.

The detailed statistics of TED3 are presented in Figure 2. Figure 2a depicts the ratio of tooth area to image area for both the training and test sets, revealing a significant variation in the mask ratio of teeth ranging from 0 to above 0.3 (refer to Figure 3 for examples with different mask ratios of teeth). The TED3 dataset demonstrates remarkable diversity across its training and validation sets, as evidenced by variations in the mask ratio of teeth. This metric serves as a reflection of both the quantity and size of teeth captured within the images. Encompassing a wide array of conditions such as metal artifacts, missing teeth, misalignment issues, and cases without dental abnormalities, this dataset encapsulates a comprehensive spectrum of dental health scenarios observed across different age demographics, including children, adults,

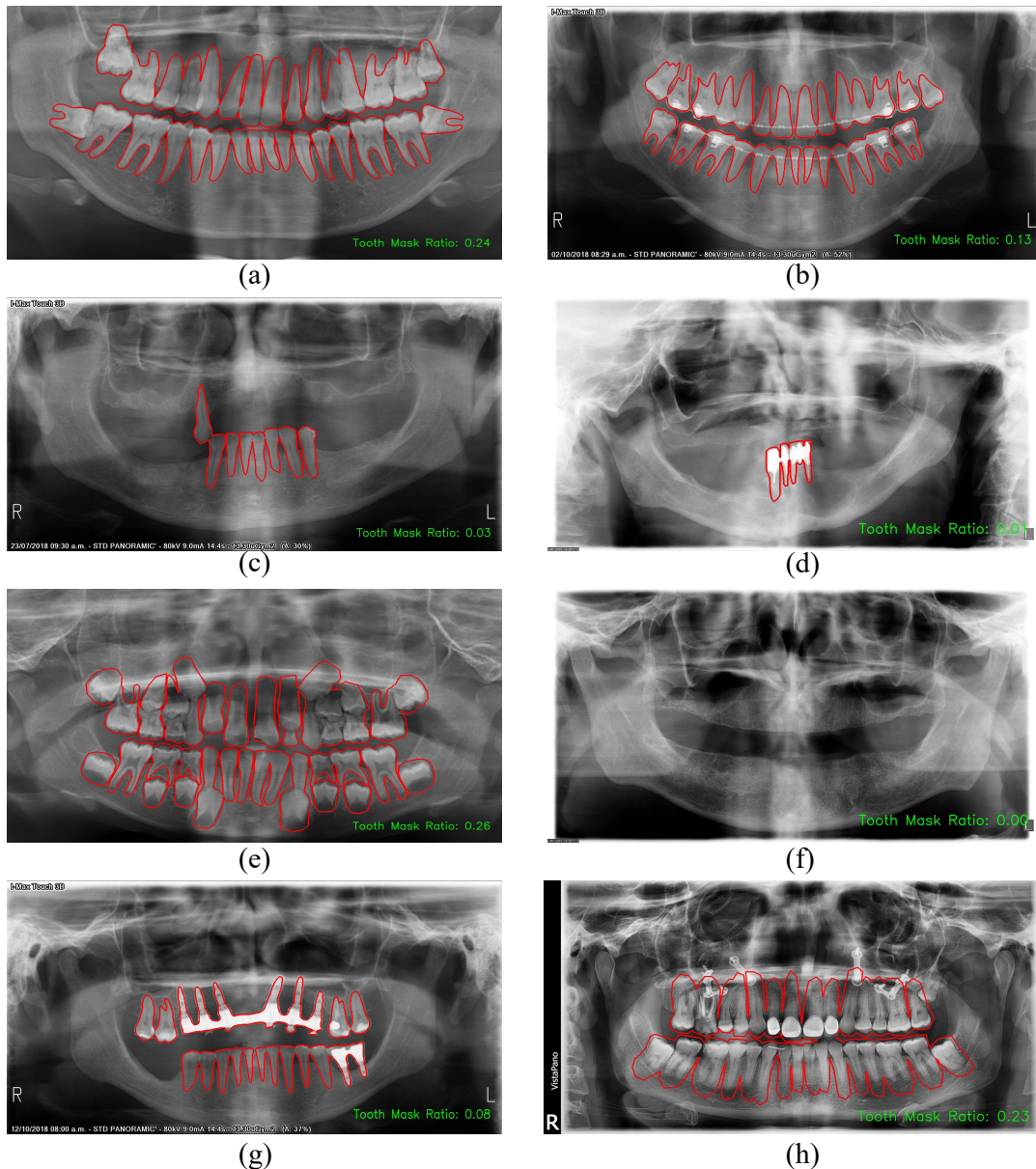


Figure 3: The examples of TED3-labelled dataset in the test set. The Tooth Mask Ratio indicates the ratio of tooth area to image area. We only visualize the contours of masks for a better view.

and the elderly. Consequently, models trained on this dataset are highly likely to exhibit robust generalization capabilities and mitigate the risk of overfitting to single-center-specific characteristics. Figure 2b illustrates the distribution of image sizes and quantities in the TED3-labeled dataset.

## 5. Experiments and Discussion

We conduct extensive comparisons with a range of stage-of-the-art (SOTA) methods and numerous vision mamba variants, demonstrating the superiority of our T-Mamba and achieving new stage-of-the-art results in terms of 2D & 3D tooth segmentation tasks. Besides, we also did sufficient ablation studies on Tim block for proving the effectiveness of each components.

## 5.1 Experiment Settings

### 5.1.1 Dataset

**3D CBCT Dataset.** The 3D CBCT dataset used in our study is collected from a large-scale CBCT dataset released by Cui et al., 2022. This large-scale dataset is used for segmentation and reconstruction of individual teeth and alveolar bone, and it consists of 4938 CBCT scans from 15 different centers in China with varying data distributions. However, only partial data has been released due to the privacy issues and regulation polices in hospitals. The data setting in our study is identical with Zhong et al., 2024, which 129 scans are used in total, dividing into a training set of 103 scans and a test set of 26 scans. The physical resolution of these scans is isotropic resolution, varying from 0.2 to 0.4  $mm^3$ . Some samples are showed in Figure 4.

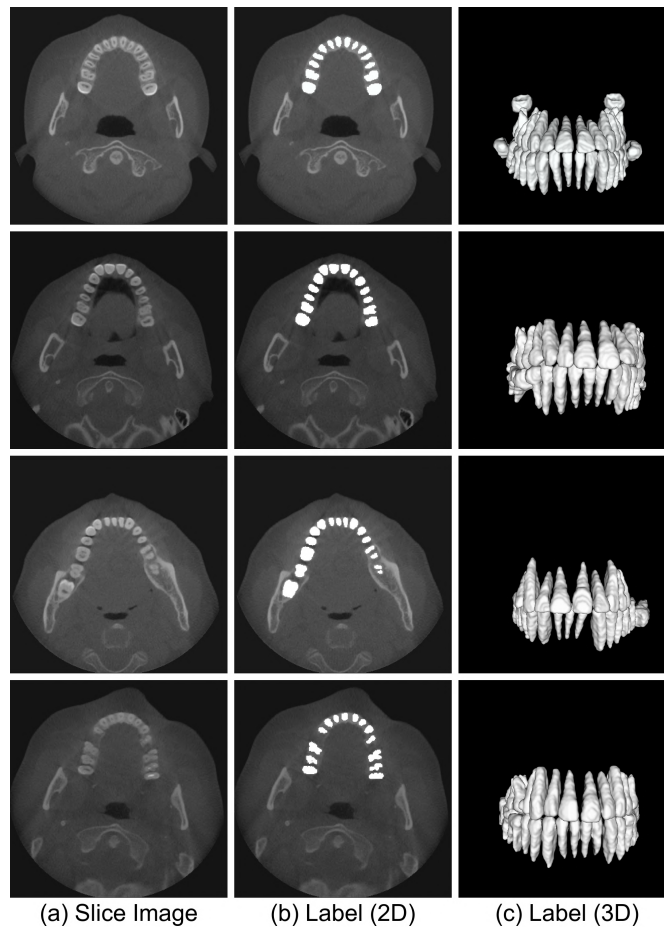


Figure 4: The 3D CBCT tooth dataset samples.

**2D TED3 Dataset.** Our proposed TED3 dataset is also used for the evaluation of our framework T-Mamba. The detailed description of this dataset has been mentioned in Sec. 4.

### 5.1.2 Implementation Details

**Experiments on 3D CBCT data.** The image pre-processing and data augmentation is strictly the same as Zhong et al., 2024. We resample each 3D image to a uniform voxel spacing of  $0.5 \times 0.5 \times 0.5mm$  and then randomly crop every image to  $160 \times 160 \times 96$  size for model inputs. The training process incorporates the AdamW optimizer with betas set to (0.9, 0.999), a momentum of 0.8, a ReduceLROnPlateau learning rate scheduler, an initial learning rate of  $5e-3$ , and a weight

decay of  $5e-5$ . Following the configuration in Zhong et al., 2024, T-Mamba undergo training from scratch for 20 epochs. Five evaluation metrics were employed to assess the network’s performance, including Dice Similarity Coefficient (DSC), Intersection over Union (IoU), Mean Intersection over Union (mIoU), Accuracy (ACC), Hausdorff Distance (HD), Average Symmetric Surface Distance (ASSD), and Surface Overlap (SO).

**Experiments on 2D X-ray data.** The color jittering and image rotation are utilized as data augmentations in the training stage. The image is resized to  $640 \times 1280$  before feeding to the network. The batch size is 16 and the AdamW optimizer is employed. The T-Mamba is trained for a total of 30 epochs with an initial learning rate of 0.0075 and weight decay of 0.00001, and the MultiStepLR strategy is used to tune the learning rate. Three metrics were employed to assess the model’s performance including Dice Similarity Coefficient (DSC), Intersection over Union (IoU), and Accuracy (ACC). All experiments are conducted using pyTorch on four NVIDIA V100 GPUs.

## 5.2 Quantitative and Qualitative Comparisons

### 5.2.1 Comparisons with the state-of-the-arts on 3D tooth CBCT

Table 2: Comparison results of different methods on the 3D CBCT tooth dataset. The best results are in bold.  $\uparrow$  means higher values are better,  $\downarrow$  means lower values are better. Results for most methods are taken from PMFSNet3D.

Method	FLOPs(G) $\downarrow$	Params(M) $\downarrow$	HD(mm) $\downarrow$	ASSD(mm) $\downarrow$	IoU(%) $\uparrow$	SO(%) $\uparrow$	DSC(%) $\uparrow$
UNet3D Çiçek et al., 2016	2223.03	16.32	113.79	22.40	70.62	70.72	36.67
DenseVNet Gibson et al., 2018	23.73	0.87	8.21	1.14	84.57	94.88	91.15
AttentionUNet3D Oktay et al., 1804	2720.79	94.48	147.10	61.10	52.52	42.49	64.08
DenseVoxelNet L. Yu et al., 2017	402.32	1.78	41.18	3.88	81.51	92.50	89.58
MultiResUNet3D Ibtehaz, 2019	1505.38	17.93	74.06	8.17	76.19	81.70	65.45
UNETR Hatamizadeh et al., 2022	229.19	93.08	107.89	17.95	74.30	73.14	81.84
SwinUNETR Hatamizadeh et al., 2021	912.35	62.19	82.71	7.50	83.10	86.80	89.74
TransBTS Wenxuan et al., 2021	306.80	33.15	29.03	4.10	82.94	90.68	39.32
nnFormer H.-Y. Zhou et al., 2023	583.49	149.25	51.28	5.08	83.54	90.89	90.66
3D UX-Net Lee et al., 2022	1754.79	53.01	108.52	19.69	75.40	73.48	84.89
PMFSNet3D Zhong et al., 2024	15.14	0.63	5.57	0.79	84.68	95.10	91.30
SegMamba	2254.30	67.36	3.95	0.6347	86.60	98.07	92.75
<b>T-Mamba (Ours)</b>	<b>25.43</b>	<b>1.04</b>	<b>1.18</b>	<b>0.42</b>	<b>88.31</b>	<b>97.53</b>	<b>93.60</b>
	-	-	<b>-4.39</b>	<b>-0.37</b>	<b>+3.63</b>	<b>+2.43</b>	<b>+2.30</b>

To evaluate the performance of our T-Mamba on the 3D tooth CBCT data, we comprehensively compare it with several state-of-the-art (SOTA) 3D networks spanning a range of neural architectures. These networks includes the UNet3D and its variants (MultiResUNet3D, AttentionUNet3D and PMFSNet3D), the DenseVNet and its variants (DenseVoxelNet), the transformer-based networks like UNETR, SwinUNETR, TransBTS, nnFormer, as well as 3D UX-Net, and vision mamba architecture like SegMamba. Table 2 demonstrates the comparisons in terms of the accuracy and computational complexity. Overall, T-Mamba achieves the best results in all metrics compared to current state-of-the-art methods, and it outperforms the previous SOTA method PMFSNet3D from accuracy perspectives by a large margin. More specifically, T-Mamba reduces the Hausdorff Distance (HD) by **4.39 mm** and the Average Symmetric Surface Distance (ASSD) by **0.37 mm**. Additionally, T-Mamba enhances the Intersection over Union (IoU) by **3.63%**, the Similarity Overlap (SO) by **2.43%**, and the Dice Similarity Coefficient

(DSC) by **2.30%**. T-Mamba’s superior performance can be attributed to its innovative integration of shared dual positional encoding and frequency-based features into the vision mamba architecture, along with a gate selection unit that adaptively combines spatial and frequency domain features, enabling it to better handle long-range dependencies and enhance feature representation in 3D CBCT tooth segmentation tasks. Figure 5 presents a qualitative comparison on a variety of teeth CBCT slices. Green boxes are used to highlight specific areas of interest, particularly regions where segmentation differences between models are more pronounced. It is evident that T-Mamba excels particularly well in handling more complex cases compared to other methods, especially in scenarios involving significant structural anomalies. Figure 6 shows a qualitative comparison on 3D tooth CBCT data segmentation.

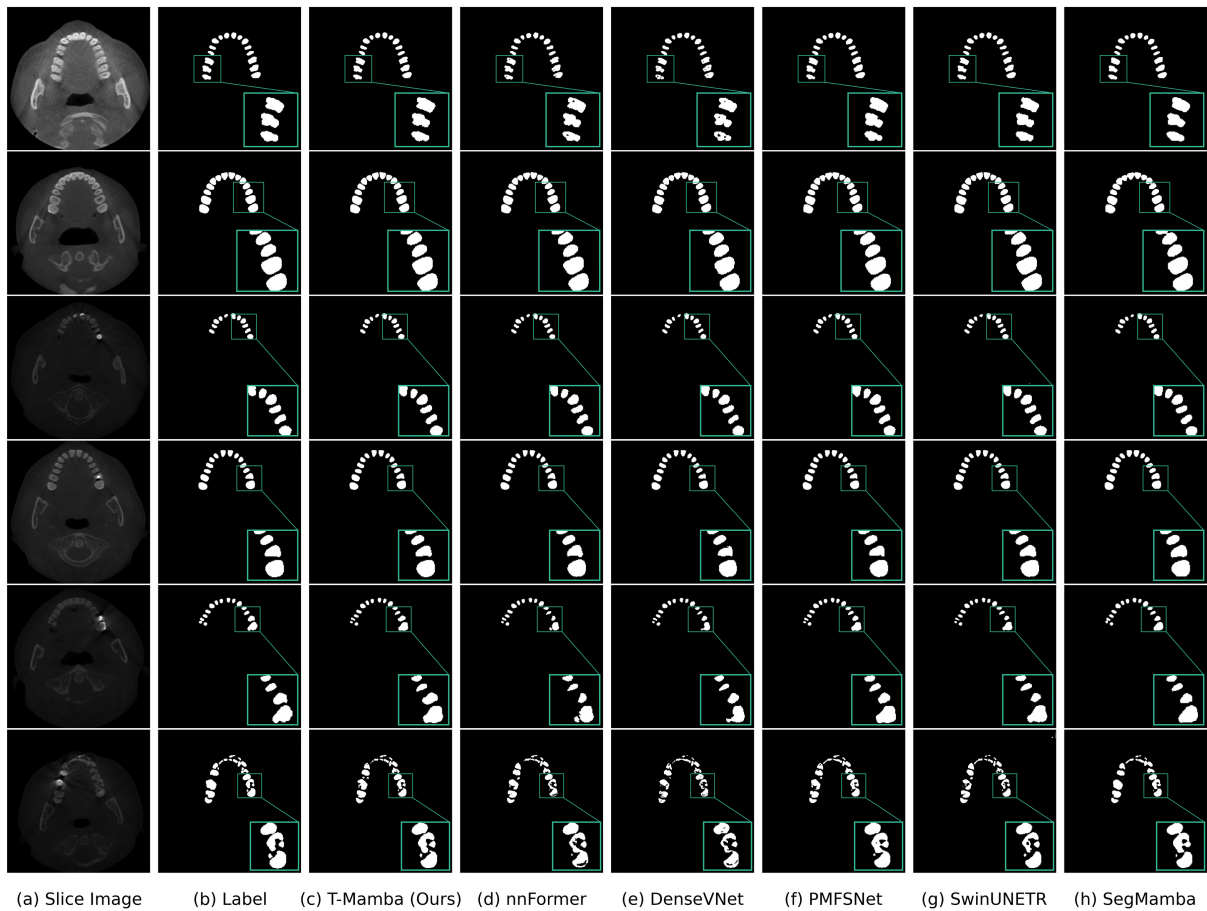


Figure 5: Visual Evaluation of T-Mamba Against State-of-the-Art Methods on 3D CBCT tooth

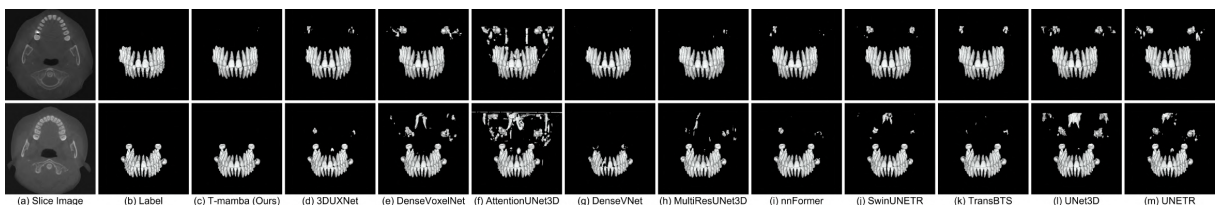


Figure 6: Visual Evaluation of T-Mamba Against State-of-the-Art Methods on 3D CBCT tooth

Table 3: Comparison results of different methods on the TED3 dataset

Method	IoU(%) $\uparrow$	DSC(%) $\uparrow$	ACC(%) $\uparrow$	Params(M) $\downarrow$
UNet	80.67	87.89	96.42	31.04
Attention-UNet	80.63	87.66	96.43	34.88
BCDU-Net	80.04	87.42	96.22	18.45
CE-Net	81.00	87.92	96.42	29.00
CPF-Net	81.51	88.30	96.52	43.27
CKD-Net	77.52	84.97	95.65	59.34
PMFSNet2D	81.31	88.15	96.51	0.99
MaskDINO	80.41	87.49	96.29	52.0
GEM	81.43	88.06	96.42	21.6
SwinUMamba	79.78	87.32	96.29	59.88
Ours	81.52	88.25	96.55	0.68
Ours + pseudo-label	82.41	88.77	96.78	0.68

### 5.2.2 Comparisons with the state-of-the-arts on TED3 dataset

We also evaluate the performance of our T-Mamba on the TED3 dataset by comparing it with several state-of-the-art (SOTA) 2D networks designed for tooth segmentation on panoramic radiographs. These networks encompass a variety of architectures, including UNet and its variants (Attention-UNet, BCDU-Net), CNN-based models (CE-Net, CPF-Net, CKD-Net, BiseNetv2, PMFSNet2D), transformer-based models (MaskDINO, GEM), and SwinUMamba. Table 3 demonstrates the comparisons in terms of accuracy and model complexity. It can be shown that our T-Mamba consistently achieves the highest accuracy across all metrics on the TED3 dataset (**81.52%** IoU, **88.25%** DSC, **96.55%** ACC), and the performance could be further enhanced by introducing the unlabelled data. Notably, our approach achieves these superior results while maintaining significantly fewer parameters. Specifically, our model utilizes only 0.68M parameters, substantially fewer than most competing models. These findings underscore that our method not only achieves state-of-the-art accuracy on the TED3 dataset but does so with exceptional efficiency, highlighting its potential for practical applications in dental image analysis.

Figure 7 and Figure 8 showcase a comparison of tooth segmentation results from the test set in TED3 dataset using different state-of-the-art models. These samples present typical panoramic dental X-ray images showing a full view of the upper and lower jaws, and some more challenging case with multiple missing teeth. The comparison includes results from (a) PMFSNet, (b) GEM, (c) SwinUMamba, (d) T-Mamba (our proposed method), and (e) Ground Truth. The segmentation results are overlaid in red on the original grayscale X-ray images. All methods perform relatively well on normal cases, with T-Mamba providing the segmentation most similar to the Ground Truth, especially in capturing the detailed contours of individual teeth and maintaining consistency across the entire dental arch. Regarding the teeth missing cases, various methods show different levels of accuracy, with T-Mamba being the most accurate one in segmenting the remaining teeth and properly identifying the toothless areas.

## 5.3 Ablation study

### 5.3.1 The architecture components.

We conduct experiments on 3D CBCT dataset to show the effectiveness of our proposed components in Tim block by adding them one at a time, which is shown in Table 4. First and foremost,

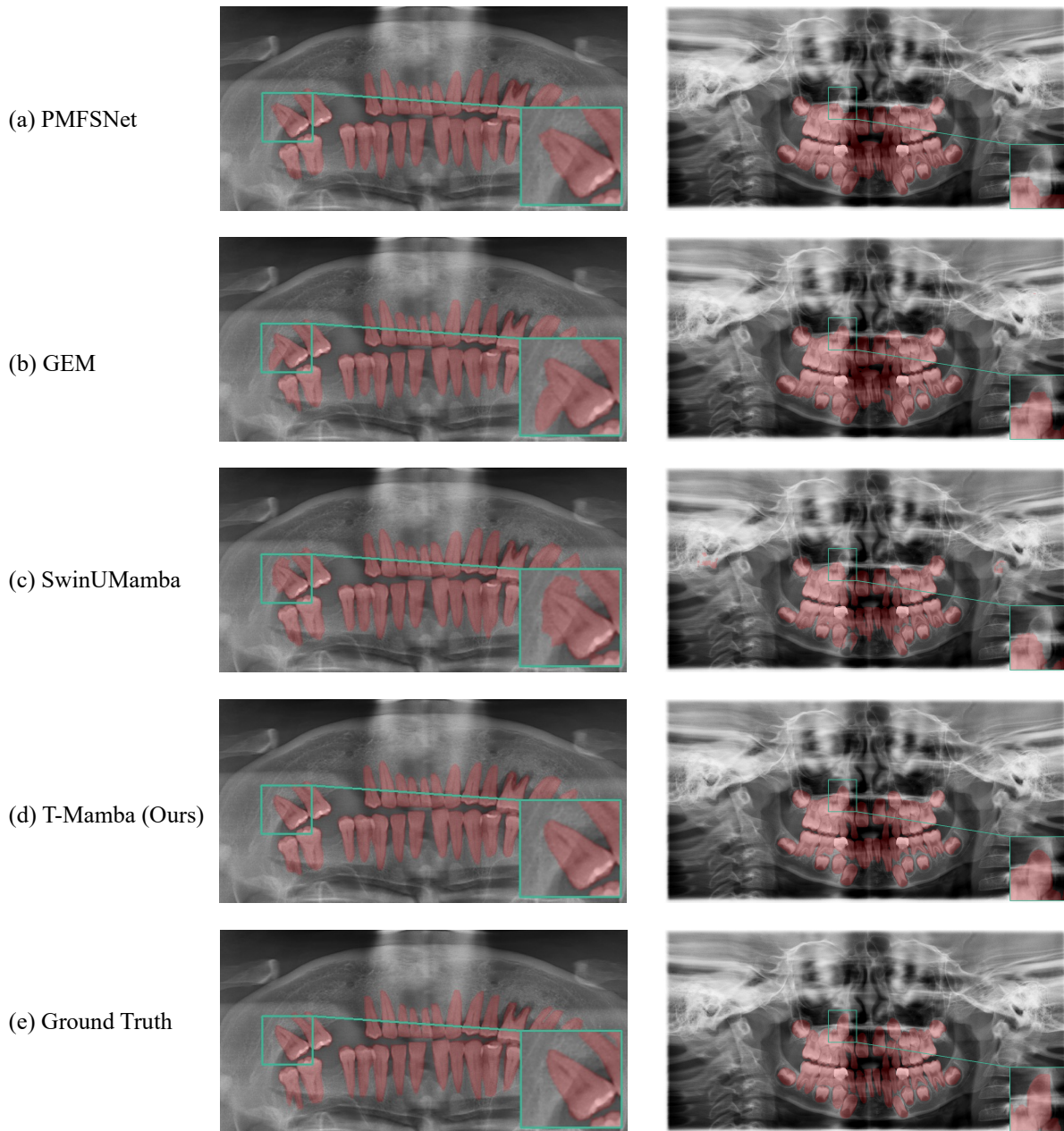


Figure 7: Qualitative Evaluation of T-Mamba Against State-of-the-Art Methods on typical panoramic images on TED3 test set.

we directly add vanilla Vim block into DenseVNet for introducing the global feature relationship modeling with linear complexity. The metric IoU, SO, DSC improve by 2.79%, 0.93%, 1.89%, respectively; but the metric HD and ASSD get worse by 1.32 and 0.11mm, respectively. This phenomenon indicates that the Vim block which could capture the long-range dependency from image features is beneficial to tooth CBCT segmentation while still exists some shortcomings. To further enhance the performance of Vim block, we introduce three components: 1) Shared bi-positional encoding compensation; 2) Frequency-based bandpass filtering; 3) Gated selection unit.

Regarding the positional encoding compensation, all metrics except HD get worse when only using the pre-position embedding which is inserted before norm operation in Tim block. On the other hand, only the metric ASSD and SO are improved when utilizing the post-position embedding which is inserted in gate selection unit. To our surprised, the shared bi-position em-

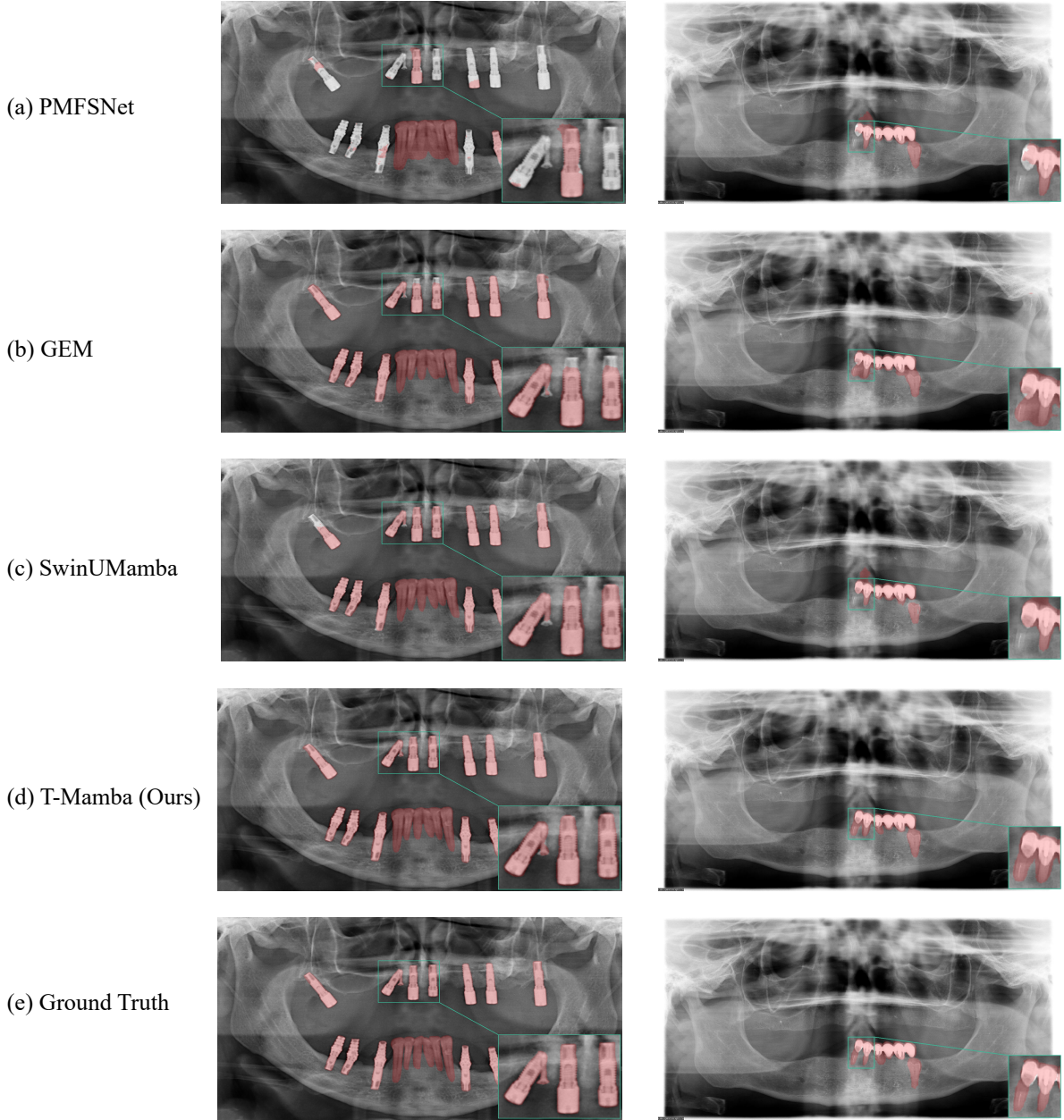


Figure 8: Qualitative Evaluation of T-Mamba Against State-of-the-Art Methods on teeth missing cases on TED3 test set.

bedding could bring significant improvements in all metrics, especially for HD and ASSD metrics. These three experiments show that the shared bi-position encoding is crucial for compensating the loss of positional information during the reshape operations of input and output, and can improve segmentation accuracy without introducing extra model parameters. Afterwards, we add the residual connection from input sequence to output sequence, and this step can bring slight increases in all metrics. We also leverage the frequency-based bandpass filtering to extract the distinctive feature representation in the frequency domain. There is a small rise in the metric IoU and DSC. Ultimately, the gate selection unit is added to adaptively fuse three kinds of features and this unit dramatically increase the metric IoU, SO, DSC. To sum up, our proposed Tim block enhances the metrics IoU, SO, DSC by 3.74%, 2.65%, 2.45%, respectively, and reduces the distance HD and ASSD by 7.03mm and 0.72mm, respectively, compared with DenseVNet baseline. Besides, our Tim block achieves higher results compared with Vim block.



Table 4: The ablation study of our Tim block.  $\uparrow$  means higher values are better,  $\downarrow$  means lower values are better.

Method	HD(mm) $\downarrow$	ASSD(mm) $\downarrow$	IoU(%) $\uparrow$	SO(%) $\uparrow$	DSC(%) $\uparrow$
DenseVNet	8.21	1.14	84.57	94.88	91.15
+ <b>Vim</b>	9.53	1.25	87.36	95.81	93.04
+ Pre Pos	7.89	1.79	87.00	95.35	92.80
+ Post Pos	10.65	1.00	87.10	96.23	92.87
+ <b>Shared bi-Pos</b>	1.22	0.59	87.65	96.79	93.20
+ <b>Residual Connection</b>	<b>1.10</b>	<b>0.39</b>	87.95	97.48	93.40
+ <b>FFT Bandpass Filtering</b>	1.18	0.67	88.05	97.26	93.47
+ <b>Gate Selection Unit</b>	1.18	0.42	<b>88.31</b>	<b>97.53</b>	<b>93.60</b>

### 5.3.2 The threshold of bandpass filtering.

We conduct extensive experiments to search the best thresholds for the high and low frequency of the bandpass filtering in Tim block, which is shown in Table 5. We find that the metrics IoU, SO, and DSC achieve the highest results when the values of high and low frequency thresholds are 0.9 and 0.1, respectively. In addition, the metrics HD and ASSD get lowest distance when these two thresholds are setting as 0.6 and 0.4, respectively. We select 0.9 and 0.1 thresholds for the high and low frequency as our default settings for other experiments.

Table 5: The ablation experiments on thresholds for the high and low frequency of the bandpass filtering in Tim block. The best results are in bold.  $\uparrow$  means higher values are better,  $\downarrow$  means lower values are better.

Low Threshold	High Threshold $\downarrow$	HD(mm) $\downarrow$	ASSD(mm) $\downarrow$	IoU(%) $\uparrow$	SO(%) $\uparrow$	DSC(%) $\uparrow$
0.1	0.9	1.18	0.42	<b>88.31</b>	<b>97.53</b>	<b>93.60</b>
0.2	0.8	1.18	0.41	87.77	97.16	93.28
0.3	0.7	1.20	0.53	87.81	97.14	93.31
0.4	0.6	<b>1.16</b>	<b>0.34</b>	87.91	97.49	93.35
0.5	0.5	1.25	0.50	87.71	97.12	93.324

### 5.4 The effect of Gated Selection Unit.

The Gated Selection Unit in Tim block is to adaptively fuse two features in spatial domain (both forward and backward directions) and one feature in frequency domain. We visualize the average proportions of these three different features on three feature-scales shown as in Figure 9 (a) and the proportions on three specific feature-scales shown as in Figure 9 (b-d) for all validation scans. In Figure 9 (a), we can observe that the forward feature, the backward feature, and frequency feature approximately occupy 41%, 28%, 31%, respectively. This could also prove that the features in frequency domain are more essential than backward feature in spatial domain. However, the proportions of these three features vary greatly in different feature-scales. For instance, in the first feature scale which belongs to low-level features, the percentage of backward feature is obviously larger than other two features. Nonetheless, the percentage of forward feature is the highest in the third feature scale which belongs to high-level features, and the the proportions of of these three features are nearly equivalent in the second feature scale.

Hence, we can draw the conclusion that our proposed Gated Selection Unit has the ability

to integrate two features in spatial domain and one feature in frequency domain adaptively, thus the model can extract more fine-grained and robust features.

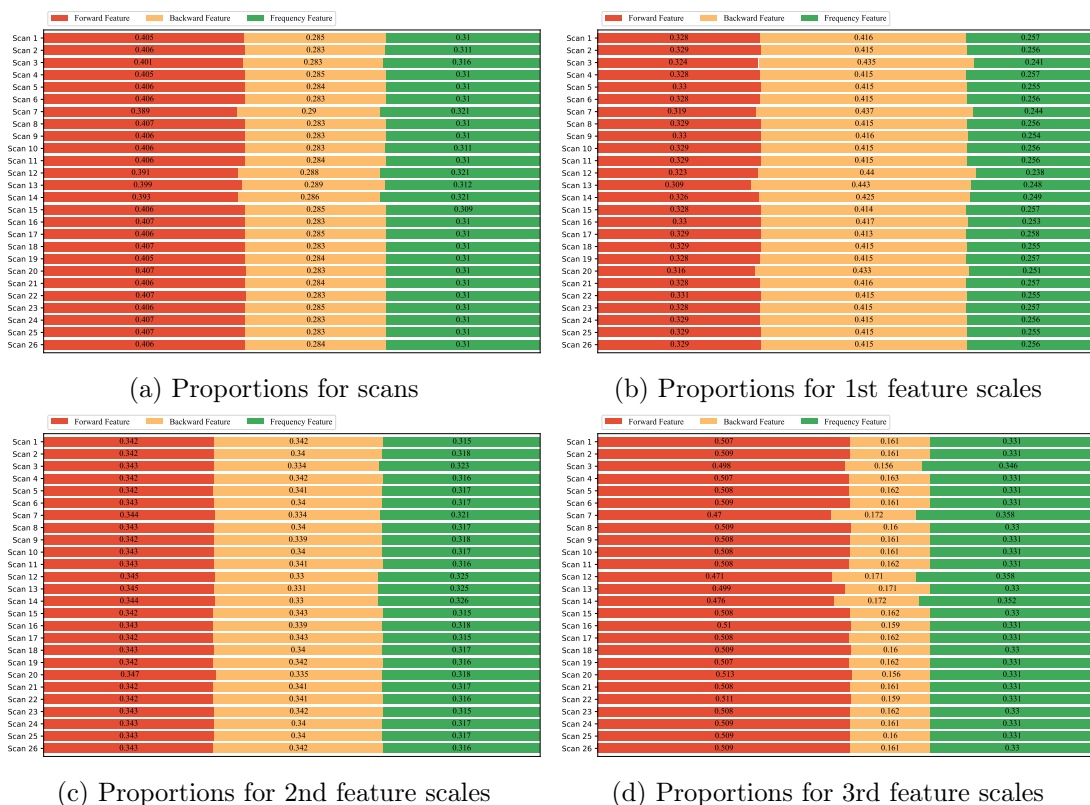


Figure 9: Four subfigures in two rows and two columns

## 5.5 Mamba v.s. Self-Attention.

T-Mamba endows the DenseVNet with the ability of global dependency modeling through the Tim module. We compared the effects of the vanilla self-attention module and our proposed Tim module directly added to the DenseVNet on the tooth CBCT dataset. As shown in Table 6, our Tim module greatly exceeds the popular self-attention module in terms of accuracy and inference speed, proving the effectiveness and efficiency of the Tim module in extracting long-range dependency of medical images.

Table 6: The ablation experiments on two global dependency modeling operations, Mamba and Self-Attention. “Time” refer to the inference time per CBCT data. The best results are in bold.  $\uparrow$  means higher values are better,  $\downarrow$  means lower values are better.

Method	HD(mm) $\downarrow$	ASSD(mm) $\downarrow$	IoU(%) $\uparrow$	SO(%) $\uparrow$	DSC(%) $\uparrow$	Time (min) $\downarrow$
DenseVNet + Self-Attn	48.04	6.78	84.07	83.79	90.08	3.96
<b>DenseVNet + Tim (ours)</b>	<b>1.18</b>	<b>0.42</b>	<b>88.31</b>	<b>97.53</b>	<b>93.60</b>	<b>2.42</b>

## 5.6 Visualization of the Grad-CAM.

We used the Grad-CAM Selvaraju et al., 2017 visualization approach to compare the feature map before and after the Tim operation, and it can be observed in Figure 10. Our Tim module assigns higher weights to the area of the tooth thanks to the strength of the global dependency

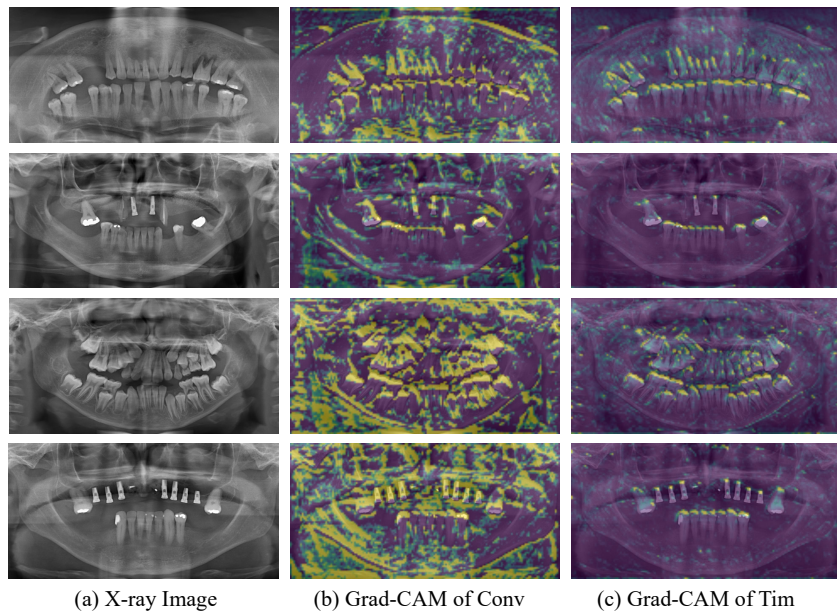


Figure 10: Grad-CAM visualizations on four dental X-ray images. The first column (a) shows the original X-ray images, the second column (b) presents the Grad-CAM visualizations generated by a convolution operation, and the third column (c) shows the Grad-CAM visualizations using our Tim module.

modeling inherited in Tim module, highlighting the regions in the image that are most important for the model’s predictions.

## 6. Conclusion

We have proposed T-Mamba to achieve global and local visual context modeling for tooth segmentation. Thanks to the proposed Tim block that integrates shared positional encoding and frequency-based features into vision mamba, we address limitations in spatial position preservation and feature enhancement in frequency domain for medical images which are of high noise and low contrast. Extensive experiments demonstrate that T-Mamba achieves new SOTA results on the public tooth CBCT dataset, showing that Tim has great potential to be the next-generation feature extractor for efficient long-range dependency modeling in biomedical image analysis. We also propose a public teeth large-scale 2D X-Ray dental dataset, TED3, and our model outperforms previous SOTA methods in a large margin on TED3 dataset. Hoping this dataset can be served as a valuable asset for propelling the application of artificial intelligence in the field of dentistry

In future works, we endeavor to explore the self-supervised learning, such as mask image modeling pretraining, in conjunction with our proposed Tim block for tooth CBCT and X-ray perception tasks. We anticipate that this advancement in technology will further propel the evolution of modern digital dentistry.

## References

- Abdi, A. H., Kasaei, S., & Mehdizadeh, M. (2015). Automatic segmentation of mandible in panoramic x-ray. *Journal of Medical Imaging*, 2(4), 044003–044003.

- ailkes, S. (2023a). Strongtoothdata. <https://www.kaggle.com/datasets/strickailkes/strongtoothdata>
- ailkes, S. (2023b). Toothdata. <https://www.kaggle.com/datasets/strickailkes/toothdata>
- Almalki, A., & Latecki, L. J. (2023). Self-supervised learning with masked image modeling for teeth numbering, detection of dental restorations, and instance segmentation in dental panoramic radiographs. *Proceedings of the IEEE/CVF Winter Conference on Applications of Computer Vision*, 5594–5603.
- Azad, R., Bozorgpour, A., Asadi-Aghbolaghi, M., Merhof, D., & Escalera, S. (2021). Deep frequency re-calibration u-net for medical image segmentation. *Proceedings of the IEEE/CVF International Conference on Computer Vision*, 3274–3283.
- Chen, Z., Chen, S., & Hu, F. (2023). Cta-unet: Cnn-transformer architecture unet for dental cbct images segmentation. *Physics in Medicine & Biology*, 68(17), 175042.
- Çiçek, Ö., Abdulkadir, A., Lienkamp, S. S., Brox, T., & Ronneberger, O. (2016). 3d u-net: Learning dense volumetric segmentation from sparse annotation. *Medical Image Computing and Computer-Assisted Intervention–MICCAI 2016: 19th International Conference, Athens, Greece, October 17–21, 2016, Proceedings, Part II 19*, 424–432.
- Cui, Z., Fang, Y., Mei, L., Zhang, B., Yu, B., Liu, J., Jiang, C., Sun, Y., Ma, L., Huang, J., et al. (2022). A fully automatic ai system for tooth and alveolar bone segmentation from cone-beam ct images. *Nature communications*, 13(1), 2096.
- Cui, Z., Li, C., Chen, N., Wei, G., Chen, R., Zhou, Y., Shen, D., & Wang, W. (2021). Tsegnet: An efficient and accurate tooth segmentation network on 3d dental model. *Medical Image Analysis*, 69, 101949.
- Cui, Z., Li, C., & Wang, W. (2019). Toothnet: Automatic tooth instance segmentation and identification from cone beam ct images. *Proceedings of the IEEE/CVF conference on computer vision and pattern recognition*, 6368–6377.
- Dosovitskiy, A., Beyer, L., Kolesnikov, A., Weissenborn, D., Zhai, X., Unterthiner, T., Dehghani, M., Minderer, M., Heigold, G., Gelly, S., et al. (2020). An image is worth 16x16 words: Transformers for image recognition at scale. *arXiv preprint arXiv:2010.11929*.
- Gao, Y., Huang, J., Sun, X., Jie, Z., Zhong, Y., & Ma, L. (2024). Matten: Video generation with mamba-attention. *arXiv preprint arXiv:2405.03025*.
- Gibson, E., Giganti, F., Hu, Y., Bonmati, E., Bandula, S., Gurusamy, K., Davidson, B., Pereira, S. P., Clarkson, M. J., & Barratt, D. C. (2018). Automatic multi-organ segmentation on abdominal ct with dense v-networks. *IEEE transactions on medical imaging*, 37(8), 1822–1834.
- Haghanifar, A., Majdabadi, M. M., Haghanifar, S., Choi, Y., & Ko, S.-B. (2023). Paxnet: Tooth segmentation and dental caries detection in panoramic x-ray using ensemble transfer learning and capsule classifier. *Multimedia Tools and Applications*, 82(18), 27659–27679.
- Hatamizadeh, A., Nath, V., Tang, Y., Yang, D., Roth, H. R., & Xu, D. (2021). Swin unetr: Swin transformers for semantic segmentation of brain tumors in mri images. *International MICCAI Brainlesion Workshop*, 272–284.
- Hatamizadeh, A., Tang, Y., Nath, V., Yang, D., Myronenko, A., Landman, B., Roth, H. R., & Xu, D. (2022). Unetr: Transformers for 3d medical image segmentation. *Proceedings of the IEEE/CVF winter conference on applications of computer vision*, 574–584.
- He, K., Gkioxari, G., Dollár, P., & Girshick, R. (2017). Mask r-cnn. *Proceedings of the IEEE international conference on computer vision*, 2961–2969.

- Hou, S., Zhou, T., Liu, Y., Dang, P., Lu, H., & Shi, H. (2023). Teeth u-net: A segmentation model of dental panoramic x-ray images for context semantics and contrast enhancement. *Computers in Biology and Medicine*, 152, 106296.
- Hung, K. F., Ai, Q. Y. H., Wong, L. M., Yeung, A. W. K., Li, D. T. S., & Leung, Y. Y. (2022). Current applications of deep learning and radiomics on ct and cbct for maxillofacial diseases. *Diagnostics*, 13(1), 110.
- Hung, K. F., Yeung, A. W. K., Bornstein, M. M., & Schwendicke, F. (2023). Personalized dental medicine, artificial intelligence, and their relevance for dentomaxillofacial imaging. *Dentomaxillofacial Radiology*, 52(1), 20220335.
- Hung, K., Montalvao, C., Tanaka, R., Kawai, T., & Bornstein, M. M. (2020). The use and performance of artificial intelligence applications in dental and maxillofacial radiology: A systematic review. *Dentomaxillofacial Radiology*, 49(1), 20190107.
- Ibtehaz, M. M., Nabil. (2019). Rethinking the u-net architecture for multimodal biomedical image segmentation. *arXiv*.
- Jang, T. J., Kim, K. C., Cho, H. C., & Seo, J. K. (2021). A fully automated method for 3d individual tooth identification and segmentation in dental cbct. *IEEE transactions on pattern analysis and machine intelligence*, 44(10), 6562–6568.
- Kanwal, M., Ur Rehman, M. M., Farooq, M. U., & Chae, D.-K. (2023). Mask-transformer-based networks for teeth segmentation in panoramic radiographs. *Bioengineering*, 10(7), 843.
- Lee, H. H., Bao, S., Huo, Y., & Landman, B. A. (2022). 3d ux-net: A large kernel volumetric convnet modernizing hierarchical transformer for medical image segmentation. *arXiv preprint arXiv:2209.15076*.
- Li, L., Liu, Q., Shi, X., Wei, Y., Li, H., & Xiao, H. (2024). Ucfiltersnet: Cross-filtering transformer-based network for ct image segmentation. *Expert Systems with Applications*, 238, 121717.
- Li, Z., Li, D., Xu, C., Wang, W., Hong, Q., Li, Q., & Tian, J. (2022). Tfns: A cnn-transformer hybrid network for medical image segmentation. *International Conference on Artificial Neural Networks*, 781–792.
- Liang, D., Zhou, X., Wang, X., Zhu, X., Xu, W., Zou, Z., Ye, X., & Bai, X. (2024). Pointmamba: A simple state space model for point cloud analysis. *arXiv preprint arXiv:2402.10739*.
- Lin, S., Hao, X., Liu, Y., Yan, D., Liu, J., & Zhong, M. (2023). Lightweight deep learning methods for panoramic dental x-ray image segmentation. *Neural Computing and Applications*, 35(11), 8295–8306.
- Liu, C., Chen, K., Chen, B., Zhang, H., Zou, Z., & Shi, Z. (2024). Rscama: Remote sensing image change captioning with state space model. *IEEE Geoscience and Remote Sensing Letters*.
- Liu, J., Yang, H., Zhou, H.-Y., Xi, Y., Yu, L., Yu, Y., Liang, Y., Shi, G., Zhang, S., Zheng, H., et al. (2024). Swin-umamba: Mamba-based unet with imagenet-based pretraining. *arXiv preprint arXiv:2402.03302*.
- Liu, Y., Tian, Y., Zhao, Y., Yu, H., Xie, L., Wang, Y., Ye, Q., & Liu, Y. (2024). Vmamba: Visual state space model. *arXiv preprint arXiv:2401.10166*.
- Loop, H. I. T. (2023). Teeth segmentation on dental x-ray images. <https://doi.org/10.34740/KAGGLE/DSV/5884500>
- Ma, J., Li, F., & Wang, B. (2024). U-mamba: Enhancing long-range dependency for biomedical image segmentation. *arXiv preprint arXiv:2401.04722*.

- Maaz, M., Shaker, A., Cholakkal, H., Khan, S., Zamir, S. W., Anwer, R. M., & Shahbaz Khan, F. (2022). Edgenext: Efficiently amalgamated cnn-transformer architecture for mobile vision applications. *European Conference on Computer Vision*, 3–20.
- MICCAI. (2023a). Dentex challenge 2023: Dental enumeration and diagnosis on panoramic x-rays. <https://dentex.grand-challenge.org/>
- MICCAI. (2023b). Miccai 2023 challenges: Sts-tooth segmentation task based on 2d panoramic images. <https://tianchi.aliyun.com/competition/entrance/532086/information>
- Momeni, M. (2023). Dental radiography analysis and diagnosis dataset. <https://www.kaggle.com/datasets/imtkaggleteam/dental-radiography>
- Nguyen, E., Goel, K., Gu, A., Downs, G., Shah, P., Dao, T., Baccus, S., & Ré, C. (2022). S4nd: Modeling images and videos as multidimensional signals with state spaces. *Advances in neural information processing systems*, 35, 2846–2861.
- Noranian, A. (2023). Tooth decay. <https://www.kaggle.com/datasets/alinoranianesfahani/tooth-decay>
- Oktaç, O., Schlemper, J., Folgoc, L. L., Lee, M., Heinrich, M., Misawa, K., Mori, K., McDonagh, S., Hammerla, N. Y., Kainz, B., et al. (2018). Attention u-net: Learning where to look for the pancreas. arXiv 2018. *arXiv preprint arXiv:1804.03999*.
- Panetta, K., Rajendran, R., Ramesh, A., Rao, S. P., & Agaian, S. (2021). Tufts dental database: A multimodal panoramic x-ray dataset for benchmarking diagnostic systems. *IEEE journal of biomedical and health informatics*, 26(4), 1650–1659.
- PranavKompally. (2023). Tooth seg. <https://www.kaggle.com/datasets/pkompally/tooth-seg>
- Rajab, T. (2023). Tooth dataset. <https://www.kaggle.com/datasets/tabarkarajab/tooth-dataset>
- Ruan, J., & Xiang, S. (2024). Vm-unet: Vision mamba unet for medical image segmentation. *arXiv preprint arXiv:2402.02491*.
- Rubiu, G., Bologna, M., Cellina, M., Cè, M., Sala, D., Pagani, R., Mattavelli, E., Fazzini, D., Ibba, S., Papa, S., et al. (2023a). Teeth segmentation in panoramic dental x-ray using mask regional convolutional neural network. *Applied Sciences*, 13(13), 7947.
- Rubiu, G., Bologna, M., Cellina, M., Cè, M., Sala, D., Pagani, R., Mattavelli, E., Fazzini, D., Ibba, S., Papa, S., et al. (2023b). Teeth segmentation in panoramic dental x-ray using mask regional convolutional neural network. *Applied Sciences*, 13(13), 7947.
- Said, E., Fahmy, G. F., Nassar, D., & Ammar, H. (2004). Dental x-ray image segmentation. *Biometric Technology for Human Identification*, 5404, 409–417.
- Selvaraju, R. R., Cogswell, M., Das, A., Vedantam, R., Parikh, D., & Batra, D. (2017). Grad-cam: Visual explanations from deep networks via gradient-based localization. *Proceedings of the IEEE international conference on computer vision*, 618–626.
- Shanbhag, S. (2023). Tooth iteration4. <https://www.kaggle.com/datasets/shwetashanbhag/tooth-iteration4>
- Shehab, R. S. (2023). Tooth detection. <https://www.kaggle.com/datasets/reemalahshehab/tooth-detection>
- Sheng, C., Wang, L., Huang, Z., Wang, T., Guo, Y., Hou, W., Xu, L., Wang, J., & Yan, X. (2023). Transformer-based deep learning network for tooth segmentation on panoramic radiographs. *Journal of systems science and complexity*, 36(1), 257–272.

- Silva, B., Pinheiro, L., Oliveira, L., & Pithon, M. (2020a). A study on tooth segmentation and numbering using end-to-end deep neural networks. *2020 33rd SIBGRAPI conference on graphics, patterns and images (SIBGRAPI)*, 164–171.
- Silva, B., Pinheiro, L., Oliveira, L., & Pithon, M. (2020b). A study on tooth segmentation and numbering using end-to-end deep neural networks. *Conference on Graphics, Patterns and Images (SIBGRAPI)*.
- Tang, H., Chen, Y., Wang, T., Zhou, Y., Zhao, L., Gao, Q., Du, M., Tan, T., Zhang, X., & Tong, T. (2024). Htc-net: A hybrid cnn-transformer framework for medical image segmentation. *Biomedical Signal Processing and Control*, 88, 105605.
- Thunderpede. (2023). Dental panoramic caries segmentation dataset. <https://www.kaggle.com/datasets/thunderpede/panoramic-dental-dataset>
- Vaswani, A., Shazeer, N., Parmar, N., Uszkoreit, J., Jones, L., Gomez, A. N., Kaiser, Ł., & Polosukhin, I. (2017). Attention is all you need. *Advances in neural information processing systems*, 30.
- wasdxa. (2023). Toothdata. <https://www.kaggle.com/datasets/wasdxa/toothdata>
- Wenxuan, W., Chen, C., Meng, D., Hong, Y., Sen, Z., & Jiangyun, L. (2021). Transbts: Multimodal brain tumor segmentation using transformer. *International Conference on Medical Image Computing and Computer-Assisted Intervention, Springer*, 109–119.
- Xin, J., Wang, A., Guo, R., Liu, W., & Tang, X. (2023). Cnn and swin-transformer based efficient model for alzheimer’s disease diagnosis with smri. *Biomedical Signal Processing and Control*, 86, 105189.
- Xing, Z., Ye, T., Yang, Y., Liu, G., & Zhu, L. (2024). Segmamba: Long-range sequential modeling mamba for 3d medical image segmentation. *arXiv preprint arXiv:2401.13560*.
- Yang, Y., Xing, Z., & Zhu, L. (2024). Vivim: A video vision mamba for medical video object segmentation. *arXiv preprint arXiv:2401.14168*.
- Ye, Z., & Chen, T. (2024). P-mamba: Marrying perona malik diffusion with mamba for efficient pediatric echocardiographic left ventricular segmentation. *arXiv preprint arXiv:2402.08506*.
- Yin, Y., Xu, W., Chen, L., & Wu, H. (2023). Cot-unet++: A medical image segmentation method based on contextual transformer and dense connection. *Mathematical Biosciences and Engineering*, 20(5), 8320–8336.
- Yu, L., Cheng, J.-Z., Dou, Q., Yang, X., Chen, H., Qin, J., & Heng, P.-A. (2017). Automatic 3d cardiovascular mr segmentation with densely-connected volumetric convnets. *Medical Image Computing and Computer-Assisted Intervention- MICCAI 2017: 20th International Conference, Quebec City, QC, Canada, September 11-13, 2017, Proceedings, Part II 20*, 287–295.
- Yu, Y., She, K., & Liu, J. (2021). Wavelet frequency separation attention network for chest x-ray image super-resolution. *Micromachines*, 12(11), 1418.
- Zhai, Y., Hao, J., Gao, L., Li, X., Gao, Y., & Han, S. (2023). Simple parameter-free self-attention approximation. *arXiv preprint arXiv:2307.12018*.
- Zhang, Y., Ye, F., Chen, L., Xu, F., Chen, X., Wu, H., Cao, M., Li, Y., Wang, Y., & Huang, X. (2023). Children’s dental panoramic radiographs dataset for caries segmentation and dental disease detection. *Scientific Data*, 10(1), 380.

- Zhong, J., Tian, W., Xie, Y., Liu, Z., Ou, J., Tian, T., & Zhang, L. (2024). Pmfsnet: Polarized multi-scale feature self-attention network for lightweight medical image segmentation. *arXiv preprint arXiv:2401.07579*.
- Zhou, H.-Y., Guo, J., Zhang, Y., Han, X., Yu, L., Wang, L., & Yu, Y. (2023). Nnformer: Volumetric medical image segmentation via a 3d transformer. *IEEE Transactions on Image Processing*.
- Zhou, Y., Huang, J., Wang, C., Song, L., & Yang, G. (2023). Xnet: Wavelet-based low and high frequency fusion networks for fully-and semi-supervised semantic segmentation of biomedical images. *Proceedings of the IEEE/CVF International Conference on Computer Vision*, 21085–21096.
- Zhu, L., Liao, B., Zhang, Q., Wang, X., Liu, W., & Wang, X. (2024). Vision mamba: Efficient visual representation learning with bidirectional state space model. *arXiv preprint arXiv:2401.09417*.
- ZHYLAR. (2023). Tooth2dseg. <https://www.kaggle.com/datasets/zhy527/tooth2dseg>



## A. Dataset Source

Table 7: The list of dataset source contained in our TED3 dataset.

No.	Data Modality	Number	Data description	Source
1	2D X-ray	7000	Tooth Semantic Segmentation 3500 labelled masks & 3500 unlabelled data	MICCAI, <a href="#">2023b</a>
2	2D X-ray	116	Mandible Semantic Segmentation 116 labelled masks	Abdi et al., <a href="#">2015</a>
3	2D X-ray	1272	Abnormal Tooth Detection Classes: ‘Cavity’, ‘Fillings’, ‘Impacted Tooth’, ‘Implant’ 1272 labelled boxes	Momeni, <a href="#">2023</a>
4	2D X-ray	598	Tooth Instance Segmentation 598 labelled masks	Loop, <a href="#">2023</a>
5	2D X-ray	100	Dental caries Semantic Segmentation 100 labelled masks	Thunderpede, <a href="#">2023</a>
6	2D X-ray	2576	Abnormal Tooth Detection Classes: ‘caries’, ‘deep caries’, ‘periapical lesions’, ‘impacted teeth’ 1005 labelled boxes & 1571 unlabelled data	MICCAI, <a href="#">2023a</a>
7	2D X-ray	543	Tooth Instance Segmentation 543 labelled masks	Silva et al., <a href="#">2020b</a>
8	2D X-ray	1000	Tooth Instance Segmentation & Language description 1000 labelled masks	Panetta et al., <a href="#">2021</a>
9	2D X-ray	1978	Tooth Semantic Segmentation & Tooth Object Detection 1978 labelled data	Zhang et al., <a href="#">2023</a>
10	2D X-ray	1988	Tooth Semantic Segmentation 1988 labelled masks	ZHYLAR, <a href="#">2023</a>
11	2D X-ray	4000	Tooth Semantic Segmentation 4000 labelled masks	wasdxa, <a href="#">2023</a>
12	2D X-ray	337	panoramic radiography 337 unlabelled data	Noranian, <a href="#">2023</a>
13	2D X-ray	4473	Abnormal Tooth Detection Including 38 classes, 4473 labelled boxes	Shehab, <a href="#">2023</a>
14	2D X-ray	3772	Abnormal Tooth Instance Segmentation Including 9 classes 3772 labelled masks	PranavKompally, <a href="#">2023</a>
15	2D X-ray	125	Tooth Object Detection 125 labelled boxes	Shanbhag, <a href="#">2023</a>
16	2D X-ray	10	Tooth Semantic Detection 10 labelled masks	Rajab, <a href="#">2023</a>
17	2D X-ray	2500	Tooth Semantic Segmentation 2000 labelled masks & 500 unlabelled data	ailkes, <a href="#">2023b</a>
18	2D X-ray	3000	Tooth Semantic Detection 3000 labelled masks	ailkes, <a href="#">2023a</a>